

Communication

# Speckle Measurement for Small In-Plane Vibration Using GaAs

Jiongye Gao , Bin Zhang <sup>\*</sup>, Qibo Feng , Xu Shen, Yong Xue and Jiacheng Liu

Key Laboratory of Luminescence and Optical Information, Ministry of Education, Beijing Jiaotong University, Beijing 100044, China

\* Correspondence: bzhang@bjtu.edu.cn

**Abstract:** In this study, the measurement characteristics of speckles based on the photoinduced electromotive force (photo-emf) effect for high-frequency, small-amplitude, and in-plane vibration were theoretically and experimentally studied. The relevant theoretical models were utilized. A GaAs crystal was used as the photo-emf detector for experimental research, as well as to study the influence of the amplitude and frequency of the vibration, the imaging magnification of the measuring system, and the average speckle size of the measuring light on the first harmonic of the induced photocurrent in the experiments. The correctness of the supplemented theoretical model was verified, and a theoretical and experimental basis was provided for the feasibility of using GaAs to measure in-plane vibrations with nanoscale amplitudes.

**Keywords:** in-plane vibration; GaAs; speckle measurement; photoinduced electromotive force

## 1. Introduction

The measurement of high-frequency micro-vibrations plays a critical role in multiple areas, such as micro-electro-mechanical systems, structural health monitoring, laser ultrasonic technology, materials science, and biomedicine [1–8]. Optical measurement methods with non-contact characteristics have been widely studied and applied [7–10]. Compared with the measurement of out-of-plane vibration, where the measuring light is parallel to the vibration direction, the measurement of in-plane vibration is relatively complex because the measuring light cannot be incident on the vibration surface in the direction parallel to the in-plane vibration direction. Speckle interferometry is commonly used for in-plane displacement measurements [11–13]. However, owing to the high-speed performance limitation of charge-coupled devices in the imaging process, they cannot measure higher frequencies. In addition, there is a low tolerance for the presence of speckles in laser beams from rough vibration surfaces for some traditional laser interferometers, leading to low measurement sensitivity.

Laser interferometry based on photorefractive crystals has become a research focus because of its advantages of wavefront matching and low-frequency cutoff [14,15] and offers some potential research directions and applications with many emerging materials [16–19]. The corresponding vibration measurement methods can restrain the influence of rough surface speckles and environmental disturbances on the measurements, thereby improving the measurement sensitivity. Among them, laser interferometry based on the photoinduced electromotive force (photo-emf) effect was first reported by Stepanov et al. [20]. In this case, the photo-emf effect is usually produced by projecting a non-steady two-beam interference light pattern on a photorefractive crystal. The interference pattern is created by the interference of a probe beam scattered by the measured sample with a coherent reference beam. The vibration of this pattern subsequently produces an ac electric current in the crystal. Stepanov et al. successively conducted theoretical research on the photo-emf effects of different photorefractive materials, as well as experimental research on interferometry under external electric field modulation for out-of-plane vibration measurement [21–28].



**Citation:** Gao, J.; Zhang, B.; Feng, Q.; Shen, X.; Xue, Y.; Liu, J. Speckle Measurement for Small In-Plane Vibration Using GaAs. *Sensors* **2023**, *23*, 2724. <https://doi.org/10.3390/s23052724>

Academic Editor: Ali Passian

Received: 29 January 2023

Revised: 28 February 2023

Accepted: 1 March 2023

Published: 2 March 2023



**Copyright:** © 2023 by the authors. Licensee MDPI, Basel, Switzerland. This article is an open access article distributed under the terms and conditions of the Creative Commons Attribution (CC BY) license (<https://creativecommons.org/licenses/by/4.0/>).

Because of the non-steady characteristics of the photo-emf, as long as the beam with harmonic oscillation shines on the photorefractive material, an alternating photocurrent will be generated. This characteristic makes it possible to measure in-plane vibration with a non-interfering speckle beam. Meanwhile, due to the non-reference beam path, it has the advantage of a simple optical arrangement. Mosquera and Frejlich conducted research on the speckle pattern measurement of in-plane vibration using a BTO crystal, and they proposed that the photocurrent signal can reach a maximum value under a certain vibration amplitude [29]. Santos conducted a theoretical study on the photocurrent signal generated by a transverse-vibration-modulated speckle light incident on a GdTe:V crystal and proposed a corresponding mathematical model and the application of this photo-emf signal to evaluate the response time of the CdTe:V crystal [30–33]. Heinz and Garmire used an array of semi-insulating GaAs photoconductive sensors to detect intensity variations caused by the transverse movement of speckles [34]. Salazar conducted experimental research based on BSO crystals and analyzed the influence of speckle size on the photocurrent [35]. Bryushinin studied the strains and stresses of their measured medium, caused by mechanical vibration, using a photo-emf sensor and measured the resonant frequency of the mechanical system and the distribution of the phase modulation amplitude on the measured surface [36].

In this study, a speckle measurement method for in-plane vibration based on a GaAs crystal photo-emf was investigated. A concrete calculation of the response time was added to the corresponding theoretical model. With the GaAs crystal as the photo detector, the effects of the vibration amplitude and frequency, as well as those of the imaging magnification of the measurement system and the average speckle size of the measuring light on the induced photocurrent, were explored. The numerical simulation and experimental results were in good agreement with those of the modified theoretical model. The measurement of in-plane vibrations of nanoscale amplitude in the frequency range of thousands of hertz was achieved.

## 2. Theoretical Analysis

The photo-emf effect is a weak non-linear optical phenomenon. A photorefractive crystal is used to receive scattered light from a remotely measured object with vibration information (as shown in Figure 1). A short-circuited crystal is illuminated by a speckle pattern with a speckle size of  $d$ . When the oscillatory movement of a speckle with a certain frequency occurs, a photocurrent is generated. The photocurrent is caused by the generation of charge carrier distribution in the conduction or valence band and the formation of a space charge field in the photoionization process; the charge carrier distribution will vibrate with the optical pattern vibration. If the time required for the spatial charge field buildup of the material is significantly lower than the vibration frequency, the vibration of the photogenerated charge carrier density can be considered to occur in the static space charge field. This behavior causes a vibrational phase shift between the static space charge field and the carrier density, resulting in the generation of a non-steady-state photocurrent.

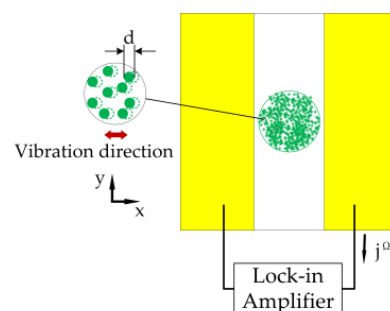


**Figure 1.** Principle of in-plane vibration measurements based on GaAs.

The intensity of a speckle pattern can be approximated by considering it as a set of Gaussian beams whose diameters are normally distributed around a diameter equal to the average speckle size. Each Gaussian beam represents a speckle particle, and the diameters of these Gaussian beams are approximately equal to the average speckle size [35]

$$d = 1.22\lambda \frac{d_i}{D_p}, \tag{1}$$

where  $d$  is the subjective speckle size,  $d_i$  is the image distance,  $\lambda$  is the wavelength, and  $D_p$  is the imaging system aperture. The light intensity of speckled particles can be expressed as

$$I = I_0 e^{-(x^2+y^2)}, \tag{2}$$

where  $w = d/2$ ,  $x = X/\sqrt{2}w$ , and  $y = Y/\sqrt{2}w$  are the coordinates normalized by the spatial coordinates  $X$  and  $Y$ , respectively;  $w = d/2$  is the Gaussian beam radius. When the measured object vibrates along the transverse direction  $x$  with amplitude  $\delta$  and angular frequency  $\Omega$ , the speckle light pattern follows the measured object vibration with angular frequency  $\Omega$  and normalized amplitude  $A = M\delta/w$ , where  $M$  is the magnification of the imaging system. Equation (2) changes to

$$I = I_0 e^{-[(x+A\sin\Omega t)^2+y^2]}, \tag{3}$$

Assuming that the material response time  $\tau_{sc}$  is significantly longer than the period of the vibration pattern  $2\pi/\Omega$  ( $\tau_{sc}\Omega \gg 1$ ), which is significantly longer than the photoelectron lifetime  $\tau$  ( $\tau\Omega \ll 1$ ), and considering cyclic frontier conditions, the average current density along the electrode space  $L$  can be obtained. The time-dependent term is as follows [30].

$$\bar{j}_{xt}(t) = \frac{j_D}{l} \int_{-\frac{l}{2}}^{\frac{l}{2}} e^{-[(x+A\sin\Omega t)^2+y^2]} \frac{E_0/E_D + \frac{\Omega}{2\pi} \int_{-\frac{2\pi}{\Omega}}^{\frac{2\pi}{\Omega}} e^{-[(x+A\sin\Omega t)^2+y^2]} (2x + 2A\sin\Omega t) dt}{\frac{\Omega}{2\pi} \int_{-\frac{2\pi}{\Omega}}^{\frac{2\pi}{\Omega}} e^{-[(x+A\sin\Omega t)^2+y^2]} dt + R_d} dx, \tag{4}$$

where  $j_D = e\mu E_D N_0$  and  $E_D = D/\mu w$ .  $\mu$  and  $D = k_B T\mu/e$  are the mobility and diffusion coefficients of the charge carriers, respectively;  $k_B$  is the Boltzmann constant;  $T$  is the absolute temperature;  $E_0 = j_0/e\mu N_0$  is the external electric field applied between the two electrodes;  $e$  is the electronic charge;  $j_0$  is the average current density along the  $x$ -direction;  $R_d = N_d/N_0$  is the dark-to-bright conductivity parameter; and  $l = L/w$ .

The photocurrent was obtained by the average current density multiplied by the area of the transverse electrode. Figure 2 shows the relationship between the amplitude and photocurrent at different high frequencies, which satisfy  $\tau_{sc}\Omega \gg 1$ .

If  $\tau_{sc}$  is not significantly longer than the vibration period  $2\pi/\Omega$ , Equation (4) should be modified to

$$\bar{j}_{xt}(t) = \frac{j_D}{l} \int_{-\frac{l}{2}}^{\frac{l}{2}} \frac{E_0/E_D + \frac{\Omega}{2\pi} \int_{-\frac{2\pi}{\Omega}}^{\frac{2\pi}{\Omega}} e^{-[(x+A\sin\Omega t)^2+y^2]} (2x + 2A\sin\Omega t) dt}{\frac{\Omega}{2\pi} \int_{-\frac{2\pi}{\Omega}}^{\frac{2\pi}{\Omega}} e^{-[(x+A\sin\Omega t)^2+y^2]} dt + R_d} e^{-[(x+A\sin\Omega t)^2+y^2]} \frac{\tau_{sc}\Omega}{\sqrt{1 + (\tau_{sc}\Omega)^2}} dx, \tag{5}$$

where  $\tau_{sc} = \frac{\epsilon\epsilon_0}{\sigma_0}$ ,  $\epsilon$  is the dielectric constant,  $\epsilon_0$  is the vacuum permittivity, and  $\sigma_0$  is the photoconductivity of the crystal [32].

The response time  $\tau_{sc}$  depends on the material itself, as well as on the incident light intensity and geometric parameters, such as the speckle size in this case. The formula of  $\tau_{sc}$  should be further clarified for sufficiently accurate photocurrent simulation. By analogy with the response time expression in the existing interferometric

measurement mode [37], the specific formula for  $\tau_{sc}$  in the speckle measurement mode can be expressed as

$$\tau_{sc}^{-1} = \frac{\sigma_0}{\varepsilon\varepsilon_0} = \frac{e\mu\alpha P_l}{\varepsilon\varepsilon_0 h\nu \left(\frac{L}{L_D}\right)^2} = \frac{\alpha P_l}{\varepsilon\varepsilon_0 \left(\frac{h\nu}{e}\right) \left(\frac{k_B T}{e}\right) \left(\frac{L}{L_D}\right)^2}, \quad (6)$$

where  $\alpha$  is the optical absorption coefficient,  $h$  is Planck's constant,  $\nu$  is the light frequency,  $P_l$  is the incident light power, and  $L_D = d/2\pi$  is the average diffusion length of photoinduced carriers.

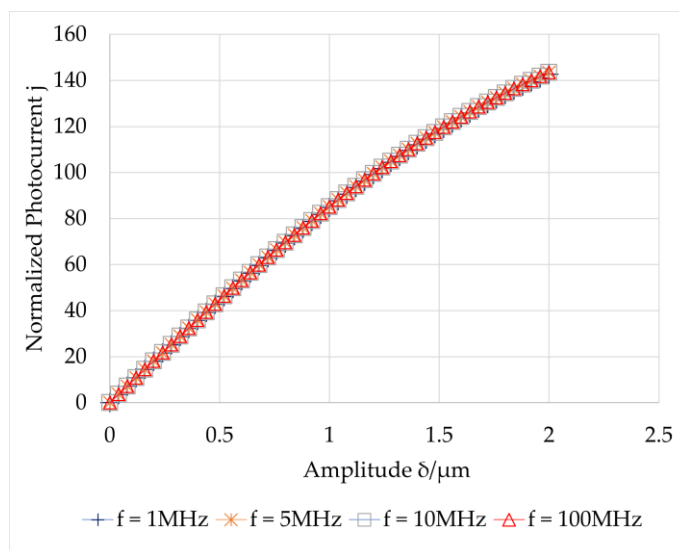


**Figure 2.** Relation between the photocurrent and vibration amplitude under  $\tau_{sc}\Omega \gg 1$ .

### 3. Numerical and Experimental Results

#### 3.1. Experimental Arrangement

The experimental setup is illustrated in Figure 3. A GaAs crystal (10 mm  $\times$  10 mm  $\times$  0.8 mm, crystal orientation [100], Molecular Technology GmbH, Berlin, Germany) with two parallel striped gold electrodes with an inter-electrode space of 2 mm on the front surface served as the detector. Its main properties include a dielectric constant of 13.1, mobility of  $5.2 \times 10^3$  cm<sup>2</sup>/(V·s), lattice constant of 0.56534 nm, and band gap of 1.4 eV. The measured object was a small and thin scattering glass plate, which was firmly adhered to a shear piezoelectric chip (PL5FBP3, Thorlabs, Newton, New Jersey, United States) and could generate transverse vibrations.

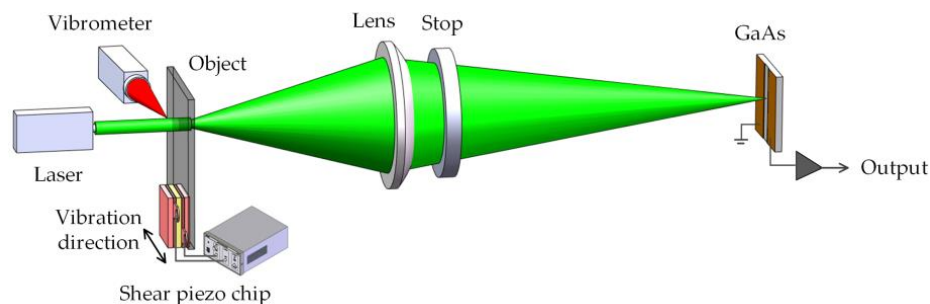


**Figure 3.** Schematic of experimental system.

The scattered glass plate was illuminated by a laser beam with a wavelength of 532 nm, 200 mW. The transmitted light was collected through a lens with a focal length of 50.8 mm, and the speckle pattern was obtained on the GaAs detector. A stop placed adjacent to the

lens was used to control the transmitted light aperture. When the vibration frequency is sufficiently high, the space charge field will not match with the photoconductive phase of GaAs, resulting in a photocurrent of the corresponding frequency. The photocurrent generated by the GaAs was measured using a lock-in amplifier. A laser vibrometer (PDV100, Polytec, Baden-Württemberg, Germany) was placed perpendicular to the optical measuring path. The measuring light hits the side of the object to obtain the corresponding out-of-plane vibration, which is also in-plane vibration. This information was used to verify the in-plane vibration and calibrate the vibration information of the measured object.

The shear piezoelectric plate was driven by 200 V at a 20 kHz sinusoidal voltage. The time-domain comparison measurement results are shown in Figure 4. Signal 1 (yellow) was obtained using PDV100, and signal 2 was obtained using GaAs (blue). The measurement results are consistent, which verifies the feasibility of the system.

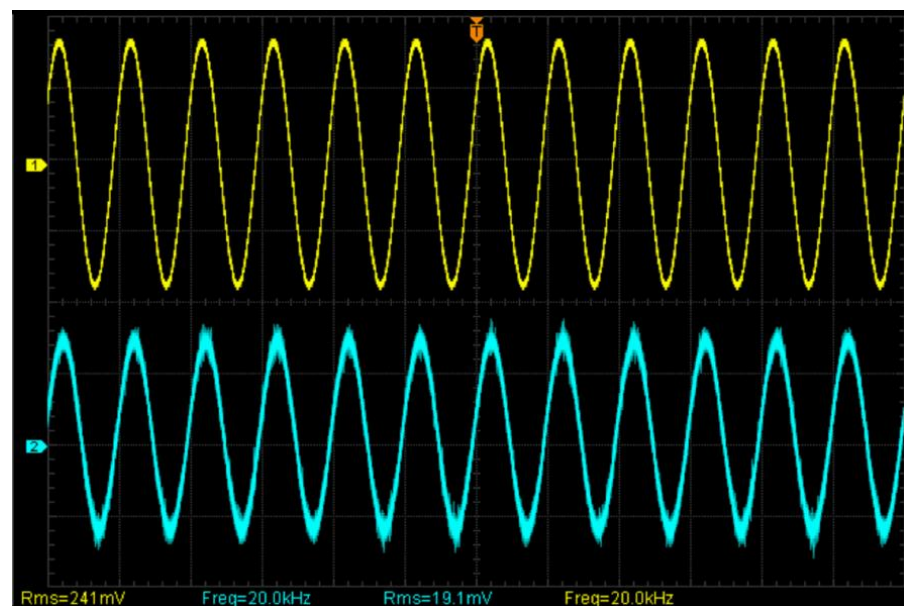


**Figure 4.** Time-domain comparison measurement results at 20 kHz.

The small in-plane vibrations at 50 kHz, 60 kHz, 70 kHz, and 75 kHz were measured separately using this system, and the frequency-domain signals were obtained using a spectrometer. The results are shown in Figure 5. It can be observed that the measured vibration frequency is consistent with the signal frequency loaded on the shear piezoelectric chip.

### 3.2. Results

The amplitude of the measured object was calibrated with the PDV100 laser vibrometer. The effects of the amplitude and frequency of the vibration, imaging magnification of the measuring system, and average speckle size of the measuring light on the induced photocurrent were explored.

#### 3.2.1. Effect of Vibration Amplitude

The aperture diameter was set to  $D_p = 50.8$  mm, the lens focal length was  $f = 50.8$  mm, and the object distance (from the diffusing element to the lens) was  $d_s = 76.81$  mm. We calculated the image distance (from the lens to the crystal) to be  $d_i = 150$  mm and the average speckle size to be  $d = 1.961$   $\mu\text{m}$ . At the same frequency, the amplitude of the measured object was changed by varying the input voltage of the shear piezoelectric chip. The measurement results and theoretical simulation results are shown in Figure 6.

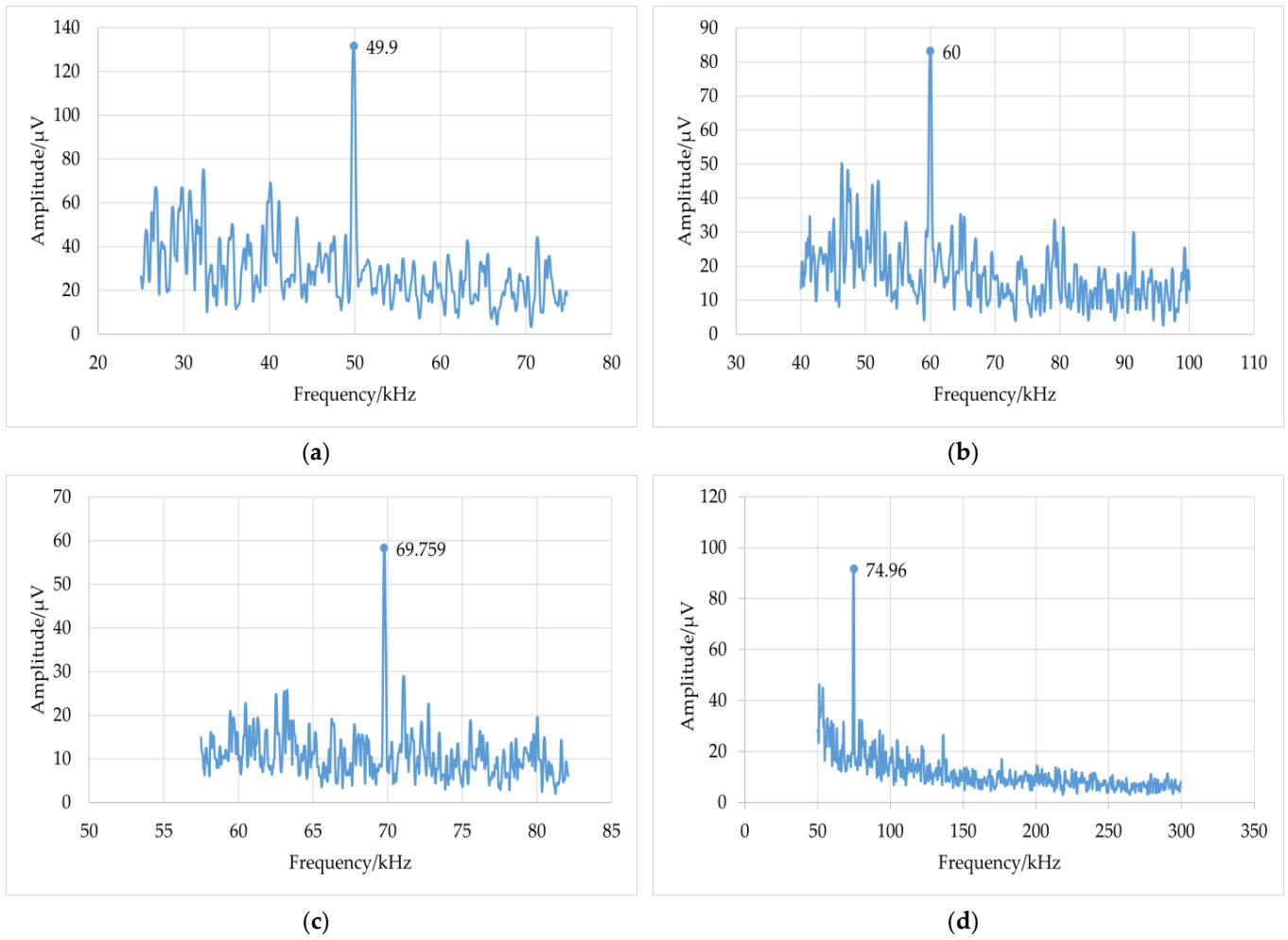


Figure 5. Measurement results of the system at different frequencies: (a) 50 kHz; (b) 60 kHz; (c) 70 kHz; (d) 75 kHz.

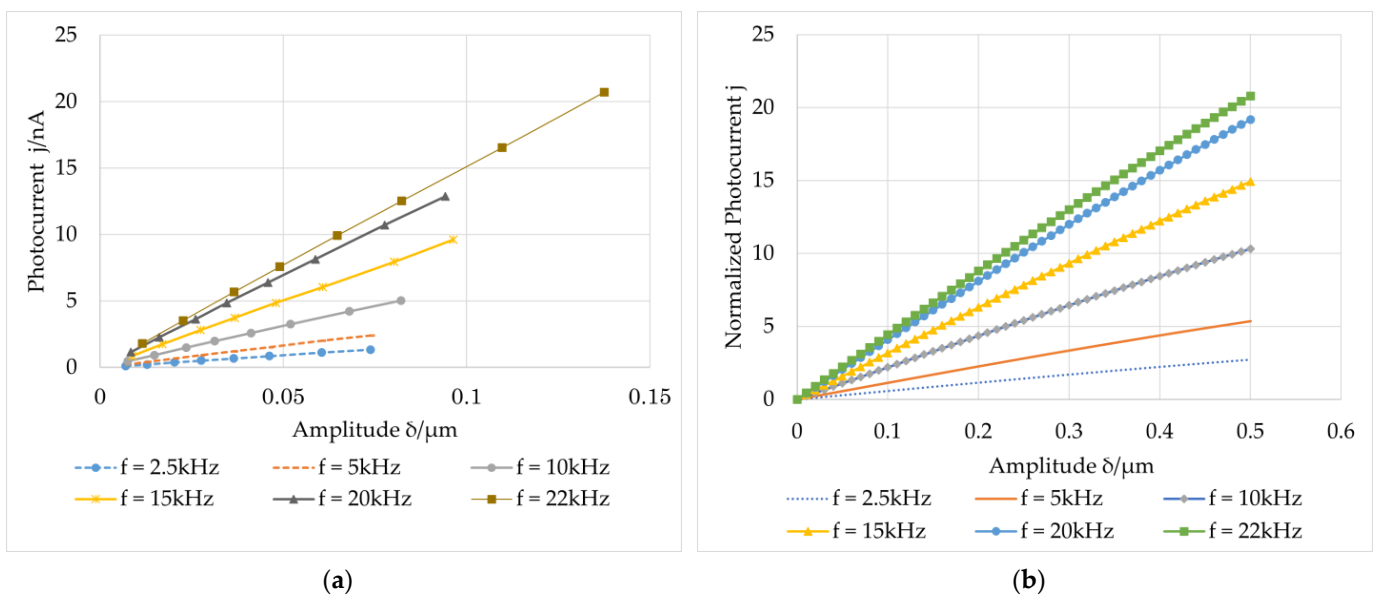
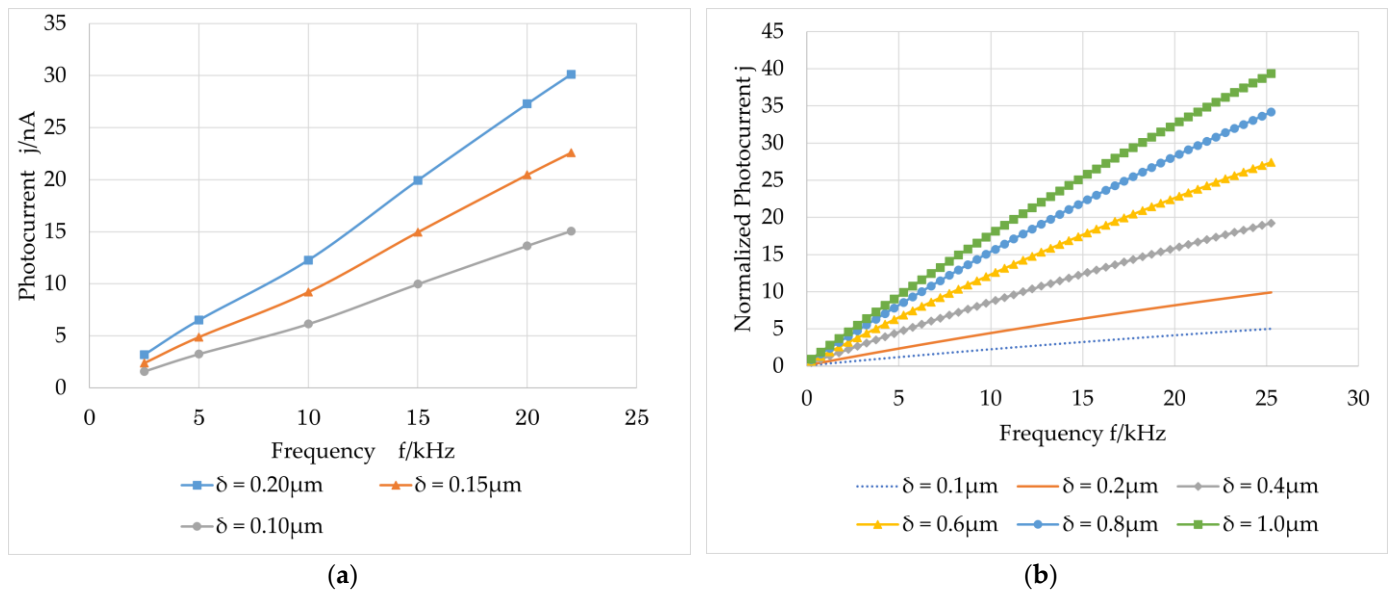


Figure 6. Relation between amplitude of the first harmonic of the photocurrent and amplitude of the vibration at different vibration frequencies: (a) experimental results; (b) theoretical simulation results.

As shown in Figure 6a, under the same vibration frequency, the induced photocurrent increases with increasing amplitude, which is the same as the simulation curve in Figure 6b. It can also be observed that the measurement system can measure in-plane vibrations of nanoscale amplitude. Although the response time is affected by the incident light intensity and the speckle size, GaAs is a fast response material.  $\tau_{sc}\Omega \gg 1$  can be met when the vibration frequency reaches several megahertz or even tens of megahertz. According to the previous statement, the photocurrent is independent of the frequency and response time in this case. For a low vibration frequency of kHz, as shown in Figure 6,  $\tau_{sc}\Omega \gg 1$  is not satisfied. When the vibration amplitude is small enough compared to the speckle size, the photocurrent is larger at higher frequencies and shows a monotonic increasing relationship.

### 3.2.2. Effect of Vibration Frequency

Under the same conditions that were applied in the previous experiment and the same voltage drive, different frequencies were loaded on the shear piezoelectric chip. Experiments and relevant theoretical simulations were performed to determine the relationship between the vibration frequency and photoinduced current, as shown in Figure 7.



**Figure 7.** Relation between the amplitude of the first harmonic of the photocurrent and vibration frequency at different vibration amplitudes: (a) experimental results; (b) theoretical simulation results.

According to Figure 7a, the photocurrent increases with increasing vibration frequency, which is the same as the tendency of the simulation results in Figure 7b. When  $\tau_{sc}\Omega \gg 1$  is not satisfied, the photocurrent will monotonously increase with the vibration frequency.

### 3.2.3. Effect of Imaging Magnification

The magnification of the imaging system was  $M = d_i/d_s = \frac{d_s}{d_s - f} = \frac{d_s - f}{f}$ , and the average speckle size was  $d = 1.22\lambda \frac{d_i}{D_p}$ . The image distance  $d_i$  must be controlled to maintain the average speckle size  $d = 1.961 \mu\text{m}$  while changing the imaging magnification.

The vibration frequency was maintained at 22 kHz, and the focal length of the lens was varied to obtain different imaging magnifications. The vibration amplitude of the speckle changed with the imaging magnification. The relationship between the photocurrent and in-plane vibration amplitude of the shear piezoelectric chip is shown in Figure 8, where the magnification  $M$  of the imaging system is 0.5, 1, and 1.952.

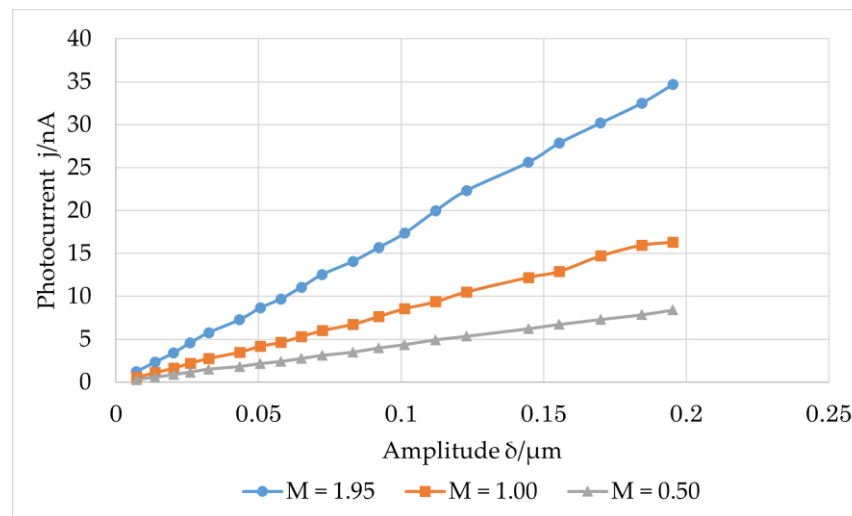


**Figure 8.** Relation between the amplitudes of the first harmonic of the photocurrent and vibration at different magnifications.

As shown in Figure 8, when the imaging magnification of the measurement system increases, the photocurrent also increases. This behavior occurs because the measured object will be magnified on the image plane after passing through the imaging system, and the amplitude of its vibration will also be magnified; thus, the photocurrent generated will also increase.

### 3.2.4. Effect of Average Speckle Size

The average speckle size was changed by changing the aperture of the imaging system. The focal length of the lens was 50.8 mm. A variable stop was placed behind the lens to change the size of the transmitted light. An optical attenuator was used to maintain the average intensity of the image surface unchanged. The experimental results obtained by adjusting the aperture to 10, 20, 30, and 40 mm are shown in Figure 9a, and the theoretical simulation results are shown in Figure 9b.

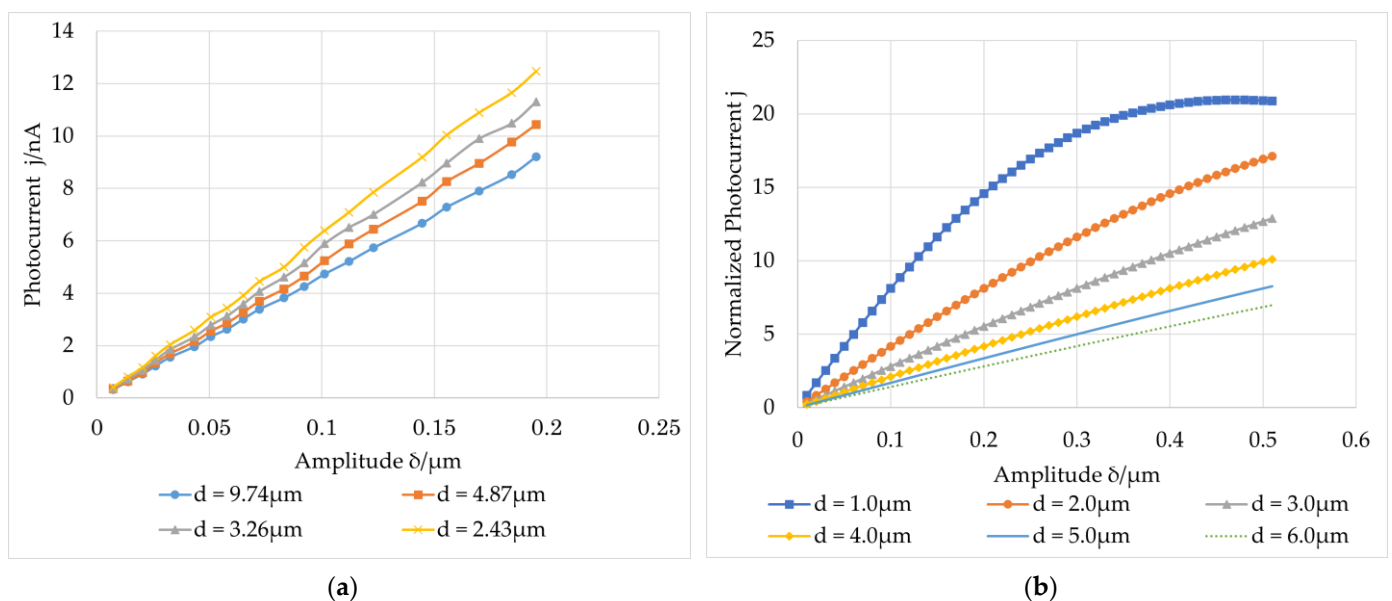


**Figure 9.** Relation curve between the amplitude of the first harmonic of the photocurrent and amplitude of the vibration at different average speckle sizes: (a) experimental results; (b) theoretical simulation results.

It can be observed that the smaller the average speckle size, the larger the output photocurrent. This finding is consistent with the simulation results shown in Figure 9b. As previously mentioned, the maximum value of  $j^{\omega}$  will appear when the amplitude  $\delta$  approaches the speckle radius  $w$  if  $\tau_{sc}\Omega \gg 1$ . However, the material response time should be considered for a case that does not meet  $\tau_{sc}\Omega \gg 1$ . The relationship between the photocurrent and amplitude in this case can be obtained by approximately estimating the response time. The photocurrent also monotonously increased with the in-plane vibration amplitude.

#### 4. Conclusions

In this study, we developed a speckle measurement method for in-plane vibrations based on the photo-emf effect of crystal GaAs. The relevant theoretical models were utilized. Through experimental and theoretical simulation, the measurement sensitivity of nanoscale vibration was confirmed and the influences of the vibration amplitude, the vibration frequency, the imaging magnification, and the average speckle size on the first harmonic of the induced photocurrent when  $\tau_{sc}\Omega \gg 1$  was not satisfied were determined. The accuracy of the supplementary response-time calculation formula was verified. This study provides a theoretical simulation and experimental basis for the application of GaAs in the measurement of in-plane, high-frequency submicron vibrations.

**Author Contributions:** Conceptualization, J.G. and B.Z.; methodology, J.G.; software, J.G.; validation, J.G., B.Z. and X.S.; formal analysis, J.G.; investigation, J.G.; resources, X.S.; data curation, J.G.; writing—original draft preparation, J.G.; writing—review and editing, B.Z. and Q.F.; visualization, J.G.; supervision, Y.X. and J.L.; project administration, B.Z.; funding acquisition, Q.F. All authors have read and agreed to the published version of the manuscript.

**Funding:** This research was funded by the National Natural Science Foundation of China (No. 51775034).

**Institutional Review Board Statement:** Not applicable.

**Informed Consent Statement:** Not applicable.

**Data Availability Statement:** Not applicable.

**Acknowledgments:** This work was supported by the National Natural Science Foundation of China (No. 51775034).

**Conflicts of Interest:** The authors declare no conflict of interest.

#### References

1. Gao, X.; Zhang, B.; Feng, Q.; Xie, X.; Yang, L. Nano-vibration measurements using the photoelectromotive force effect in the GaAs crystal. *Instrum. Exp. Tech.* **2016**, *59*, 470–475. [[CrossRef](#)]
2. Li, H.; Jiang, W.; Deng, J.; Yu, R.; Pan, Q. A Sensitive Frequency Range Method Based on Laser Ultrasounds for Micro-Crack Depth Determination. *Sensors* **2022**, *22*, 7221. [[CrossRef](#)]
3. Ghafoor, I.; Tse, P.; Rostami, J.; Ng, K.-M. Non-Contact Inspection of Railhead via Laser-Generated Rayleigh Waves and an Enhanced Matching Pursuit to Assist Detection of Surface and Subsurface Defects. *Sensors* **2021**, *21*, 2994. [[CrossRef](#)]
4. Kang, K.; Park, K. Noncontact Laser Ultrasound Detection of Cracks Using Hydrophone. *Sensors* **2021**, *21*, 3371. [[CrossRef](#)]
5. Passian, A.; Evans, P.G.; Varma, V.K.; Ferrell, T.L.; Thundat, T. Piezoresistive detection of acoustic waves. *Rev. Sci. Instrum.* **2003**, *74*, 1031–1035. [[CrossRef](#)]
6. Zaharov, V.; Farahi, R.H.; Snyder, P.; Davison, B.; Passian, A.; Blouin, B.C.C.N. Karhunen-Loeve treatment to remove noise and facilitate data analysis in sensing, spectroscopy and other applications. *Analyst* **2014**, *139*, 5927–5935. [[CrossRef](#)]
7. Yu, B.; Tola, K.D.; Lee, C.; Park, S. Improving the Ability of a Laser Ultrasonic Wave-Based Detection of Damage on the Curved Surface of a Pipe Using a Deep Learning Technique. *Sensors* **2021**, *21*, 7105. [[CrossRef](#)]
8. Choi, S.; Ota, T.; Nin, F.; Shioda, T.; Suzuki, T.; Hibino, H. Rapid optical tomographic vibrometry using a swept multi-gigahertz comb. *Opt. Express* **2021**, *29*, 16749. [[CrossRef](#)]
9. Cao, Y.; Xiong, J.; Liu, X.; Xia, Z.; Wang, W.; Yadav, N.P.; Liu, W. Sensing of ultrasonic fields based on polarization parametric indirect microscopic imaging. *Chin. Opt. Lett.* **2019**, *17*, 41702. [[CrossRef](#)]
10. Volikova, A.M.; Lobach, I.A.; Kablukov, S.I. Laser vibrometer-rangefinder based on self-sweeping fiber laser. *Opt. Express* **2022**, *30*, 22025. [[CrossRef](#)]
11. Souto Janeiro, A.; Fernández López, A.; Chimeno Manguan, M.; Pérez-Merino, P. Three-dimensional digital image correlation based on speckle pattern projection for non-invasive vibrational analysis. *Sensors* **2022**, *22*, 9766. [[CrossRef](#)]

12. Zhao, Y.; Zhang, H. Displacement measurement method based on laser self-mixing interference in the presence of speckle. *Chin. Opt. Lett.* **2020**, *18*, 51201. [[CrossRef](#)]
13. Gao, X.; Yang, L.; Wang, Y.; Zhang, B.; Dan, X.; Li, J.; Wu, S. Spatial phase-shift dual-beam speckle interferometry. *Appl. Opt.* **2018**, *57*, 414. [[CrossRef](#)] [[PubMed](#)]
14. Bryushinin, M.; Kulikov, V.; Sokolov, I.; Delaye, P.; Pauliat, G. Non-steady-state photo-EMF in semi-insulating GaAs under frequency-modulated illumination. *Europhys. Lett.* **2014**, *105*, 64003. [[CrossRef](#)]
15. Mansurova, S.; Zarate, P.M.; Rodriguez, P.; Stepanov, S.; Köber, S.; Meerholz, K. Non-steady-state photoelectromotive force effect under linear and periodical phase modulation: Application to detection of Doppler frequency shift. *Opt. Lett.* **2012**, *37*, 383–385. [[CrossRef](#)]
16. Kour, R.; Arya, S.; Verma, S.; Singh, A.; Mahajan, P.; Khosla, A. Review-recent advances and challenges in indium gallium nitride (InxGa1-xN) materials for solid state lighting. *ECS J. Solid State Sci. Technol.* **2019**, *9*, 15011. [[CrossRef](#)]
17. Young, S.-J.; Liu, Y.-H.; Shiblee, M.D.N.I.; Ahmed, K.; Lai, L.-T.; Nagahara, L.; Thundat, T.; Yoshida, T.; Arya, S.; Furukawa, H.; et al. Flexible Ultraviolet Photodetectors Based on One-Dimensional Gallium-Doped Zinc Oxide Nanostructures. *ACS Appl. Electron. Mater.* **2020**, *2*, 3522–3529. [[CrossRef](#)]
18. He, Z.; Asare-Yeboah, K.; Zhang, Z.; Bi, S. Manipulate organic crystal morphology and charge transport. *Org. Electron.* **2022**, *103*, 106448. [[CrossRef](#)]
19. He, Z.; Zhang, Z.; Bi, S. Tailoring the molecular weight of polymer additives for organic semiconductors. *Mater. Adv.* **2022**, *3*, 1953–1973. [[CrossRef](#)]
20. Stepanov, S.I.; Sokolov, I.A.; Trofimov, G.S.; Vlad, V.I.; Popa, D.; Apostol, I. Measuring vibration amplitudes in the picometer range using moving light gratings in photoconductive GaAs:Cr. *Opt. Lett.* **1990**, *15*, 1239–1241. [[CrossRef](#)]
21. Stepanov, S. Chapter 6—Photo-electromotive-force effect in semiconductors. In *Handbook of Advanced Electronic and Photonic Materials and Devices*; Singh Nalwa, H., Ed.; Academic Press: Burlington, MA, USA, 2001; pp. 205–272.
22. Stepanov, S.; Montero, P.R.; Flores, M.A.C.; Mixcoatl, J.C.; Lopez, A.A.; Carrasco, L.A.; Sanchez, M.S. Interferometric applications of GaAs adaptive photo-EMF detectors. *J. Opt. Technol.* **2002**, *69*, 428. [[CrossRef](#)]
23. Korneev, N.; Mansurova, S.; Rodriguez, P.; Stepanov, S. Fast and slow processes in the dynamics of near-surface space-charge grating formation in GaAs. *J. Opt. Soc. Am. B* **1997**, *14*, 396. [[CrossRef](#)]
24. Korneev, N.A.; Mansurova, S.S.; Stepanov, S.I.; Hall, T.J.; Powell, A.K. Non-steady-state photoelectromotive force in semiconductor photorefractive crystals biased by dc field. *J. Opt. Soc. Am. B* **1996**, *13*, 2278. [[CrossRef](#)]
25. Sokolov, I.A.; Stepanov, S.I. Detection of optical signals with high-amplitude phase modulation by adaptive photodetectors. *Appl. Opt.* **1993**, *32*, 1958–1964. [[CrossRef](#)]
26. Sokolov, I.A.; Stepanov, S.I. Non-steady-state photoelectromotive force in crystals with long photocarrier lifetimes. *J. Opt. Soc. Am. B* **1993**, *10*, 1483. [[CrossRef](#)]
27. Korneev, N.A.; Stepanov, S.I. Non-steady-state photoelectromotive force in semiconductor crystals with high light absorption. *J. Appl. Phys.* **1993**, *74*, 2736–2741. [[CrossRef](#)]
28. Korneev, N.; Stepanov, S. Measurement of Small Lateral Vibrations of Speckle Patterns Using a Non-steady-state Photo-EMF in GaAs: Cr. *J. Mod. Opt.* **1991**, *38*, 2153–2158. [[CrossRef](#)]
29. Mosquera, L.; Frejlich, J. Self-calibrating speckle photo-electromotive force for large vibration amplitude measurement. *J. Opt. A Pure Appl. Opt.* **2004**, *6*, 1001–1004. [[CrossRef](#)]
30. Dos Santos, T.O.; Launay, J.C.; Frejlich, J. Photo-electromotive-force from volume speckle pattern vibration with large amplitude. *J. Appl. Phys.* **2008**, *103*, 113104. [[CrossRef](#)]
31. Dos Santos, T.O.; Frejlich, J.; Shcherbin, K. Photo electromotive force in CdTe:Ge: Manifestation of two photorefractive centers. *Appl. Phys. B* **2010**, *99*, 701–707. [[CrossRef](#)]
32. Santos, T.; Launay, J.C.; Odoulov, S.G.; Frejlich, J. The speckle photo-electromotive force on a vanadium-doped CdTe crystal. *J. Opt. A Pure Appl. Opt.* **2008**, *10*, 104007. [[CrossRef](#)]
33. Dos Santos, T.O.; Frejlich, J.; Launay, J.C.; Shcherbin, K. Speckle photo electromotive force in CdTe:V and CdTe:Ge for measurement of vibration with large amplitude. *Appl. Phys. B* **2009**, *95*, 627–632. [[CrossRef](#)]
34. Heinz, P.; Garmire, E. Optical vibration detection with a photoconductance monitoring array. *Appl. Phys. Lett.* **2004**, *84*, 3196–3198. [[CrossRef](#)]
35. Salazar, A. Speckle photo-electromotive force in Bi12SiO20: Effect of the speckle size. *Opt. Commun.* **2013**, *298–299*, 207–212. [[CrossRef](#)]
36. Bryushinin, M.; Kulikov, V.; Petrov, A.; Sokolov, I.A.; Romashko, R.V.; Kulchin, Y.N. Non-steady-state photo-EMF interferometer for detection of mechanical oscillations in transparent scattering objects. *Appl. Opt.* **2020**, *59*, 2370. [[CrossRef](#)] [[PubMed](#)]
37. Gao, X. Study of Ultrasonic Interference Measurement Method Based on the Photoemf Effect. Doctoral Dissertation, Beijing Jiaotong University, Beijing, China, 2017.

**Disclaimer/Publisher’s Note:** The statements, opinions and data contained in all publications are solely those of the individual author(s) and contributor(s) and not of MDPI and/or the editor(s). MDPI and/or the editor(s) disclaim responsibility for any injury to people or property resulting from any ideas, methods, instructions or products referred to in the content.